











Atomistic defects as single-photon emitters in atomically thin MoS₂

Cite as: Appl. Phys. Lett. **117**, 070501 (2020); <https://doi.org/10.1063/5.0018557>

Submitted: 15 June 2020 . Accepted: 30 July 2020 . Published Online: 18 August 2020

K. Barthelmi, J. Klein , A. Hötger, L. Sigl, F. Sigger, E. Mitterreiter, S. Rey, S. Gyger , M. Lorke , M. Florian, F. Jahnke, T. Taniguchi, K. Watanabe , V. Zwiller, K. D. Jöns , U. Wurstbauer , C. Kastl , A. Weber-Bargioni, J. J. Finley , K. Müller , and A. W. Holleitner 



View Online



Export Citation



CrossMark

ARTICLES YOU MAY BE INTERESTED IN

[Room temperature infrared detectors made of PbTe/CdTe multilayer composite](#)

Applied Physics Letters **117**, 072102 (2020); <https://doi.org/10.1063/5.0018686>

[Enhancing the photoelectrical performance of graphene/4H-SiC/graphene detector by tuning a Schottky barrier by bias](#)

Applied Physics Letters **117**, 071102 (2020); <https://doi.org/10.1063/5.0012566>

[High quality three-dimensional aluminum microwave cavities](#)

Applied Physics Letters **117**, 070601 (2020); <https://doi.org/10.1063/5.0016463>

Lock-in Amplifiers
up to 600 MHz



Watch



Atomistic defects as single-photon emitters in atomically thin MoS₂

Cite as: Appl. Phys. Lett. **117**, 070501 (2020); doi: [10.1063/5.0018557](https://doi.org/10.1063/5.0018557)

Submitted: 15 June 2020 · Accepted: 30 July 2020 ·

Published Online: 18 August 2020













View Online



Export Citation



CrossMark

K. Barthelmi,^{1,2} J. Klein,^{1,2,3}  A. Hötger,^{1,2} L. Sigl,^{1,2} F. Sigger,^{1,2} E. Mitterreiter,^{1,2} S. Rey,^{1,2} S. Cyger,⁴  M. Lorke,⁵ 
M. Florian,⁵ F. Jahnke,⁵ T. Taniguchi,⁶ K. Watanabe,⁷  V. Zwiller,⁴ K. D. Jöns,⁴  U. Wurstbauer,⁸  C. Kastl,^{1,2} 
A. Weber-Bargioni,⁹ J. J. Finley,^{1,2,a)}  K. Müller,^{1,2,a)}  and A. W. Holleitner^{1,2,b)} 

AFFILIATIONS

¹Walter Schottky Institut und Physik Department, Technische Universität München, Am Coulombwall 4, 85748 Garching, Germany

²Munich Center of Quantum Science and Technology (MCQST), Schellingstr. 4, 80799 Munich, Germany

³Department of Materials Science and Engineering, Massachusetts Institute of Technology, Cambridge, Massachusetts 02139, USA

⁴KTH Royal Institute of Technology, Department of Applied Physics, Albanova University Centre, Roslagstullsbacken 21, 106 91 Stockholm, Sweden

⁵Institut für Theoretische Physik, Universität Bremen, P.O. Box 330 440, 28334, Bremen, Germany

⁶International Center for Materials Nanoarchitectonics, National Institute for Materials Science, 1-1 Namiki, Tsukuba 305-0044, Japan

⁷Research Center for Functional Materials, National Institute for Materials Science, 1-1 Namiki, Tsukuba 305-0044, Japan

⁸Institute of Physics, University of Münster, 48149 Münster, Germany

⁹Molecular Foundry, Lawrence Berkeley National Laboratory, 1 Cyclotron Road, Berkeley, California 94720, USA

^{a)}Electronic addresses: finley@wsi.tum.de and kai.mueller@wsi.tum.de

^{b)}Author to whom correspondence should be addressed: holleitner@wsi.tum.de

ABSTRACT

Precisely positioned and scalable single-photon emitters (SPEs) are highly desirable for applications in quantum technology. This Perspective discusses single-photon-emitting atomistic defects in monolayers of MoS₂ that can be generated by focused He-ion irradiation with few nanometers positioning accuracy. We present the optical properties of the emitters and the possibilities to implement them into photonic and optoelectronic devices. We showcase the advantages of the presented emitters with respect to atomistic positioning, scalability, long (microsecond) lifetime, and a homogeneous emission energy within ensembles of the emitters. Moreover, we demonstrate that the emitters are stable in energy on a timescale exceeding several weeks and that temperature cycling narrows the ensembles' emission energy distribution.

Published under license by AIP Publishing. <https://doi.org/10.1063/5.0018557>

Single-photon emitters (SPEs) are key requirements for applications in quantum information technologies,^{1–4} such as quantum computing,^{5,6} quantum communication,⁷ and boson sampling.^{8,9} SPEs can be found in numerous material systems. For three-dimensional materials, the most prominent examples comprise fluorescent atomic defects, the so-called color centers,² and semiconductor quantum dots.¹⁰ Prominent examples for color centers are N- or Si-vacancy centers in diamond,^{2,11} which can be created through chemical vapor deposition or ion implantation.² Although their single-photon emission characteristics excel at room temperature,² due to the implantation in a three dimensional system, their axial and/or lateral positioning precision is somewhat limited.^{11,12}

Recently, it was discovered that two-dimensional materials can also host SPEs,^{13–20} where strain-induced SPEs appear randomly near edges or wrinkles as it was first reported for monolayers of transition-metal dichalcogenides (TMDCs) such as WSe₂.^{13,16} Deterministically strain-induced SPEs in TMDCs could be demonstrated through nano-patterned environments even within large scale arrays.^{17–19} SPEs were also demonstrated in GaSe, in which deformations through Se clusters formed during the growth process can cause strain, and in turn, the resulting local confinement potential traps excitons.²⁰ In hexagonal boron nitride (hBN), single-photon emission is observed up to room temperature.²¹ Here, SPEs can be generated through electron beam irradiation and annealing,²² etching,²³ intentional strain,²⁴ and CVD

growth.²⁵ However, the spatial position of such SPEs is either random or semi-deterministic with a rather broad variation of emission energies.

All the described systems exhibit their own characteristics and advantageous properties of technological relevance since different applications have specific requirements. As a consequence, there are strong efforts in investigating SPE systems. An ideal SPE emits single-photons on demand with high purity, as well as high brightness and stability. Moreover, it should be precisely positioned, and the single photons emitted should be indistinguishable with a narrow ensemble distribution of emission energies.^{1,26} Furthermore, for a possible cluster state generation and memory, an engineered coupling to a spin bath is desirable.²⁷ For all such systems, a scalable approach to generate the SPEs is crucial for the use in many applications.

In this Perspective, we discuss a recently established SPE system, namely, a single atomistic defect in monolayer MoS₂,^{28,29} as a scalable approach to define SPEs with a position accuracy of about 9 nm.^{29,30} The defects show sharp optical emission lines within a narrow ensemble distribution,^{28,29} while the recombination lifetime is rather long in the range of hundreds of nanoseconds up to microseconds.²⁹ Due to the advantages of the fabrication method of a maskless patterning with a focused He-ion beam and its beneficial characteristics, the presented defects are interesting candidates to be integrated into photonic and optoelectronic devices.^{31–33} We highlight recent advances in the scalable generation of such atomistic defects in monolayer MoS₂ and discuss the optical characteristics of the photon emission, which is stable in time over several weeks. Moreover, we demonstrate that temperature cycling narrows the ensembles' emission energy distribution.

SPEs can be generated in monolayers of MoS₂ with ~ 9 nm precision through irradiation with a focused He-ion beam.³⁰ For generating high-quality optical SPEs, the MoS₂ monolayer is encapsulated in the top and bottom layer of hBN of ~ 10 nm thickness.²⁹ The encapsulation reduces the impact of ambient gases and the SiO₂/Si substrate, for example, by doping and surface roughness,^{34–36} and it reduces the effect of residues from nanofabrication.³⁵ After assembling the heterostacks, they are irradiated with He-ions [Fig. 1(a)]. This approach leads to a better optical quality of the photoluminescence (PL) of the samples with much cleaner emission lines compared to encapsulating the MoS₂ monolayers after the He-ion treatment.³⁴ In particular, the broad emission from adsorbate-related luminescence can be sufficiently suppressed in this way.²⁹ The positioning resolution is in first order limited by the nanometer sized focused ion beam of the utilized He-ion microscope (HIM, Zeiss) in combination with the backscattering radii of sputtered substrate atoms, backscattered He-ions, and secondary electrons.^{28,30,37,38} A computational scattering model predicts a radius of 8 nm for defects to be generated in MoS₂.³⁸ Very consistently, we could reveal a positioning resolution of the defects within ~ 9 nm by a combined study of HIM and scanning tunneling microscopy (STM).³⁰ The STM analysis suggests that mostly S- and Mo-monovacancies are generated by the HIM.³⁰

The He-ion irradiation generates defects with sharp emission lines at an emission energy of $E_{\text{photon}} \sim 1.75$ eV with a FWHM of ~ 28 meV at 10 K,²⁹ which is ~ 200 meV below the neutral 1s exciton X_{1s}^0 of MoS₂ measured on the same samples [Fig. 1(b)]. The luminescence of the defects dominates the overall photoluminescence spectrum at low temperatures (below ~ 100 K),²⁸ and intriguingly, it is more intense than the luminescence of the neutral free exciton (X_{1s}^0).

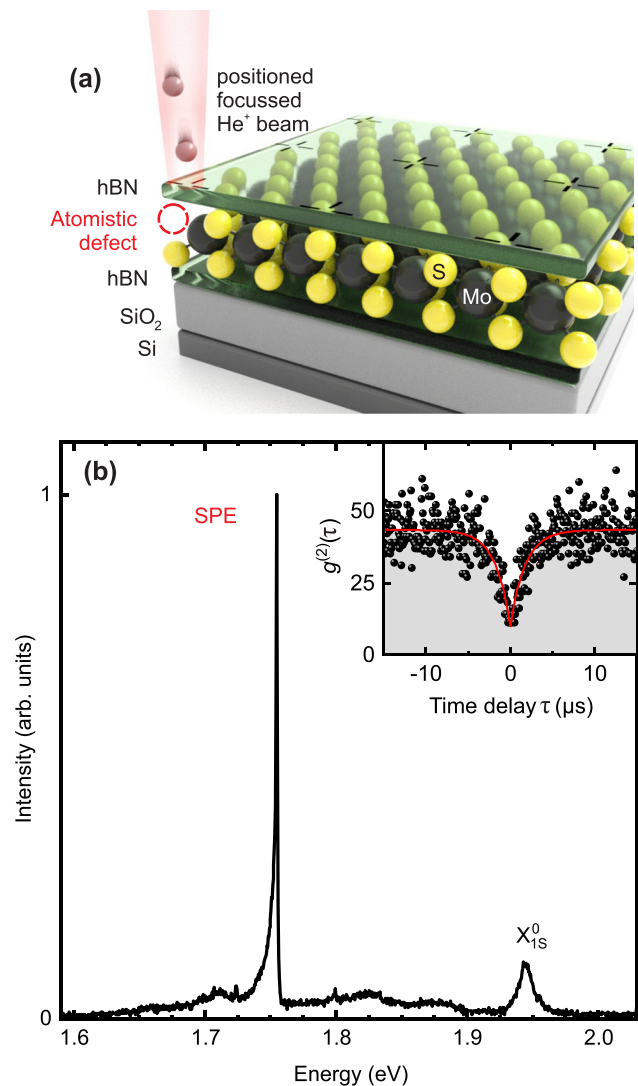


FIG. 1. Nanofabricated single-photon emitters in a monolayer of MoS₂. (a) Scheme of generating atomistic defects in an hBN/MoS₂/hBN heterostack using a focused and positioned He-ion beam in a He-ion microscope (HIM). (b) Low temperature photoluminescence spectrum of a defect that acts as a single-photon emitter (SPE). The luminescence of the SPE dominates the overall emission spectrum including the one of the neutral exciton X_{1s}^0 in MoS₂ (spot size: $\sim 1 \mu\text{m}$, $T_{\text{bath}} = 10$ K, $E_{\text{exc}} = 2.33$ eV, and $P = 0.9 \mu\text{W}$). Inset: auto-correlation function $g^{(2)}(\tau)$ of the photoluminescence stemming from one SPE ($T_{\text{bath}} = 5$ K, $E_{\text{exc}} = 1.96$ eV, and $P = 14$ nW).

The asymmetry of the emission peaks is caused by phonon interactions, most likely with LA and TA phonons, which can be effectively described by an independent boson model.²⁸

The He-ion induced defects show an antibunching behavior [inset of Fig. 1(b)], with the second-order correlation function being $g^{(2)}(0) = 0.23 \pm 0.04$ at zero time delay at 5 K.²⁹ The width of the dip in $g^{(2)}(\tau)$ gives an estimate for the recombination lifetime of $(1.73 \pm 0.15) \mu\text{s}$.²⁹ This means that the irradiation with a focused He-ion beam generates rather long-lived defect states in monolayer MoS₂.

with sharp optical emission lines and with a positioning precision of only a few nanometers.

Using the HIM, specific areas and thus local patterns on the MoS₂ samples can be irradiated in a maskless way such that for instance, defect arrays and matrices can be created [Fig. 2(a)]. A typical array of the utilized HIM is $20 \times 20 \mu\text{m}^2$, but with the help of stitching algorithms, large scale patterns can easily be exposed.³⁹

For a long-term characterization of the SPEs, we probed their optical properties during seven cooldown cycles within three months. One cooldown cycle implies cooling down a sample in a ⁴He-flow cryostat to a bath temperature of $T_{\text{bath}} = 10 \text{ K}$, which takes about 0.5–1 h, and then, the sample is continuously measured at 10 K over a period of 24–72 h. After the measurements, the sample is cycled back to room temperature without any external annealing, which takes about one day.

Figure 2(a) shows an optical micrograph of the He-ion irradiated hBN/MoS₂/hBN van der Waals heterostructure and the false color micro-photoluminescence (μ -PL) maps for the seven cooldown cycles (1–7). The maps display the spatially resolved photoluminescence of the SPE matrix spectrally integrated within the energy range of 1.7 eV–1.88 eV. As an orientation, the HIM exposure pattern is overlaid with the optical micrograph of the heterostructure and the first PL map (1) as indicated by red and black dots. A pitch of $2 \mu\text{m}$ between the exposure sites ensures a straight-forward optical inspection of each SPE. The He-ion dose and exposure time are optimized such that single SPEs are generated nearly on-demand as we have

recently demonstrated.²⁹ In the current study, we characterize exposure sites with a mean number of about 91 SPEs, with some of the sites having more than one SPE and some of them having none as will be discussed below. We find that 67% of the sites are optically active for almost all cooldown cycles. Importantly, the SPE's emission energy stays rather constant at $\sim 1.75 \text{ eV}$, which is an apparent advantage of the described atomistic SPEs in MoS₂.²⁹ To demonstrate this, we highlight two positions A and B in the first PL map [Fig. 2(a)] and show their spectra for all cooldown cycles in Figs. 2(b) and 2(c). We also observe emitters that are inactive in one cooldown cycle but are reactivated in the subsequent cooldown, which can be explained by a thermally activated redistribution of fabrication inhomogeneities, such as strain in the van der Waals heterostructure or diffusion of residues in the MoS₂/hBN interfaces. Moreover, charge carriers might be trapped in defect sites and freeze there at low temperatures. Such defects could be in close proximity to the SPEs in MoS₂ or in hBN and could easily switch the SPE on and off. In particular, at position A, the emission intensity is slightly lowered in the first, third, and fourth cooldown cycles [Fig. 2(b)], but it reappears in the second, fifth, sixth, and seventh cycles, while at position B, the corresponding SPE has a reduced brightness during the second and fourth cooldown cycles [Fig. 2(c)]; thus, we can exclude the influence of different setup alignments. In this context, we mention that changes on the microscopic scale of a localized single defect are also accompanied by changes in the delocalized free excitons. In particular, the peak position and also the ratio of the intensity between the neutral exciton at $\sim 1.95 \text{ eV}$ and the

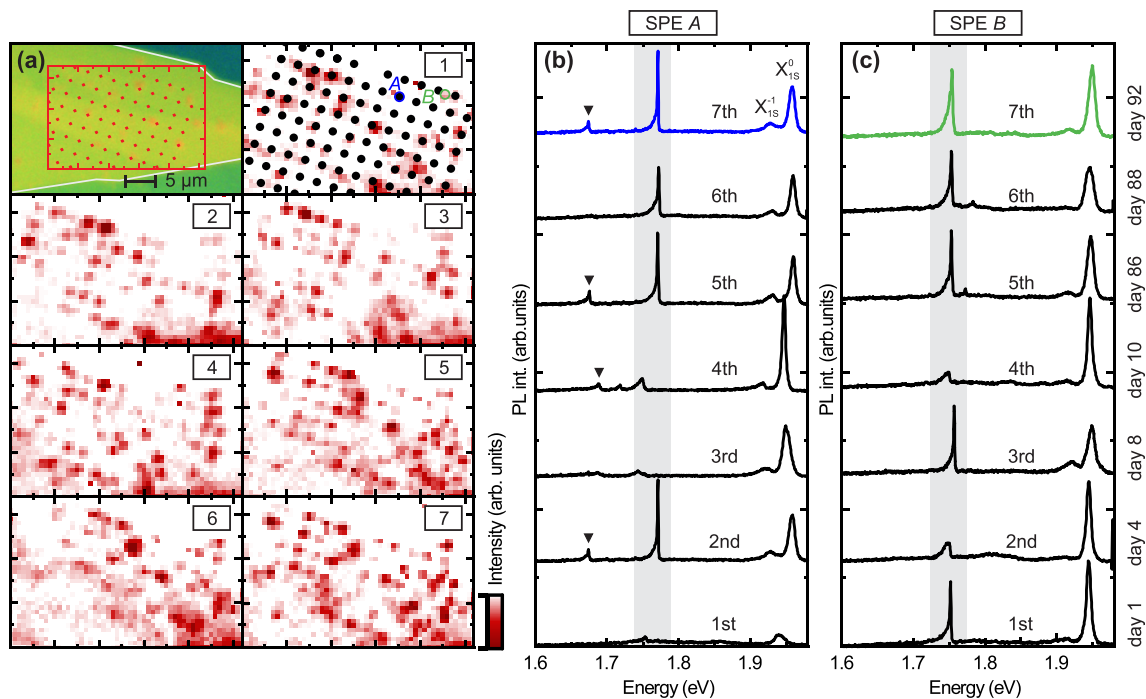


FIG. 2. Spatially localized quantum light arranged in an array. (a) Microscope image of a heterostack (white line) with red dots highlighting the position of He-ion irradiation. (1)–(7) PL maps of the sample taken after one (1) to seven (7) cooldown cycles from room temperature to $T_{\text{bath}} = 10 \text{ K}$ for the red-marked area in the microscope image. In (1), the defect array exposed by the HIM is indicated by black dots. Two positions A and B are marked by circles representing the diffraction limited laser spot diameter ($\sim 1 \mu\text{m}$). (b) and (c) PL spectra of the defect emitter at positions A and B shown for the cooldown cycles (1)–(7) and the given days of laboratory time ($T_{\text{bath}} = 10 \text{ K}$, $E_{\text{exc}} = 2.33 \text{ eV}$, and $P = 0.9 \mu\text{W}$).

negatively charged trion vary from cooldown to cooldown. The latter suggests a local variation in the charge carrier concentration, as increasing the carrier density leads to an enhancement of the formation of trions.⁴⁰

In a recent STM study,³⁰ we could resolve seven different HIM-induced defects in monolayer MoS₂ including S- and Mo-vacancies. The most common point defect in TMDCs is a chalcogen vacancy.^{30,41} Moreover, since metal defects have a much lower occurrence in the TMDCs,³⁰ the observed emission peaks at 1.75 eV most likely stem from pure sulfur vacancies without oxygen passivation.⁴¹ In our present understanding, oxygen passivated sulfur vacancies are unlikely to be responsible for the observed emission peaks, as they are also present in pristine MoS₂ without HIM treatment.³⁰ The encapsulation of MoS₂ in hBN prior to the He-ion irradiation very likely protects unsaturated dangling bonds of He-ion induced defects.²⁹ According to theory, the optically active defect state lies within the energy gap and acts effectively as an exciton trap,⁴² giving rise to exciton-like states⁴¹ that are expected to be observable as absorption features down to 1.7 eV.⁴² Due to their similar energy of occupied and unoccupied states, there is a strong hybridization between the defect states and the electronic states in the first Brillouin zone.⁴¹ Indeed, in some of the exposure sites, single peaks with a much lower intensity appear at lower emission energy additionally to the main peaks at 1.75 eV [cf. triangles in Fig. 2(b)]. However, further theoretical modeling is needed to understand such defect orbitals, their hybridization with conduction and valence band states, and their oscillator strength.^{41,42}

To demonstrate the robustness of the atomistic quantum emitters, we extract the PL spectra of each SPE within the maps of Fig. 2 with respect to their emission energy and temperature cycle. For each exposure site, one spectrum is taken and the emission peaks are fitted. Figure 3(a) shows the energy detuning ΔE between the emission of the SPE and X_{1s}^0 . Figures 3(b)–3(h) show the histograms of emission energies for all optically active quantum emitters of the cooldown cycles (1)–(7). We detect a clustering of photon emission events at ~ 195 meV, which is the main emission distribution induced by He-ion irradiation.^{28,29,43}

The distribution of the emission energies around ~ 195 meV narrows with the cooldown cycles (see Gaussian fits). Over the seven cooldown cycles, the FWHM of the distribution is reduced from above 53 ± 8 meV to about 28 ± 4 meV [Fig. 3(i)] and saturates after cooldown number three (dashed line). During all cycles, the number of active quantum emitter peaks fluctuates around a mean value of ~ 91 [Fig. 3(j)]. This number exceeds the one of the characterized and active sites ~ 61 (mean value) in the PL maps of Fig. 2(a), which is explained by multiple defects on certain exposure sites, while other sites may show even none.²⁹ The emitters outside of the fitted Gaussian distribution as in Figs. 3(a)–3(h) are the ones with much lower intensity [highlighted by triangles as in Fig. 2(b)].

The analysis of the PL maps reveals a continuous narrowing of the main emission distribution around ~ 1.75 eV after several cooldown cycles. We interpret this optimization of the ensembles' emission energy distribution by a thermally activated reduction of inhomogeneity from the movement of adsorbates between the layers in combination with strain relaxation. Particularly, with the linear thermal expansion coefficient of hBN being negative and the one of MoS₂ being positive,⁴⁴ the heterostack layers most likely get strained during cooldown, resulting in relative movement with respect to each

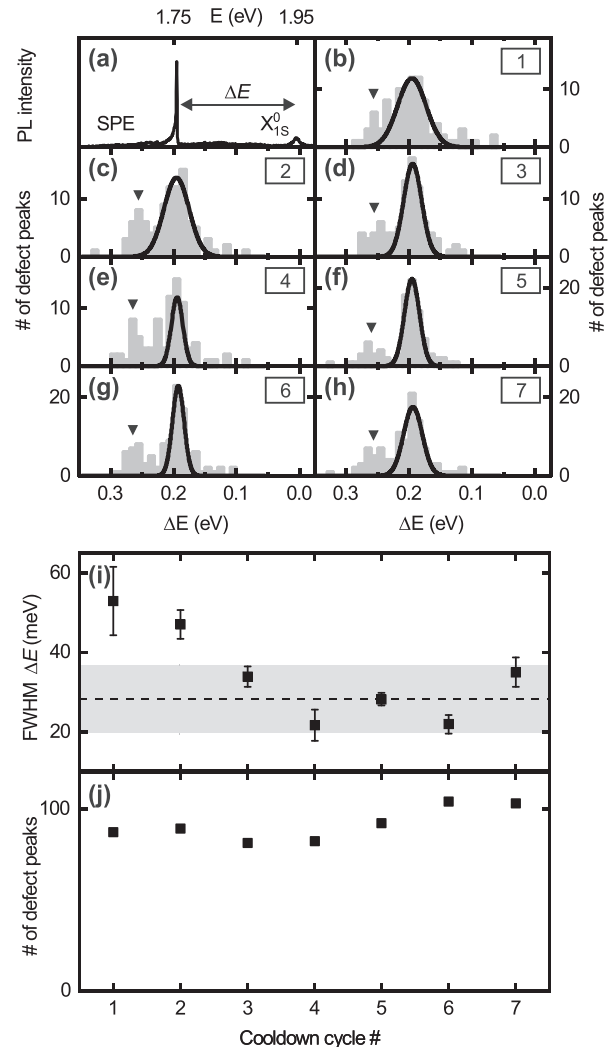


FIG. 3. Optimization of the energetic distribution of quantum emitters. (a) Typical PL spectrum of one emitter (SPE) at $T_{\text{bath}} = 10$ K. The energy detuning ΔE between the emission of the SPE and X_{1s}^0 is highlighted. (b)–(h) Probability distribution of the emission energy of ~ 91 SPEs on the heterostack depicted in Fig. 2(a) fitted by a Gaussian distribution (black) for the seven cooldown cycles (1)–(7), respectively. The number of peaks with specific emission energies with respect to the X_{1s}^0 exciton emission is depicted in gray. (i) FWHM of the Gaussian distribution of ΔE for the seven cooldown cycles. The average of the energy distribution of cooldown (5)–(7) is displayed by the dashed line. (j) The total number of fitted emission peaks for each of the seven cooldown cycles ($T_{\text{bath}} = 10$ K, $E_{\text{exc}} = 2.33$ eV, and $P = 0.9 \mu\text{W}$).

other and in a similar fashion release strain when cycling back to room temperature. In turn, adsorbates and fabrication residues very likely get diffusive and aggregate in clusters and therefore get removed from the defect locations. We point out that the number of the emission peaks is stable during the cycles [Fig. 3(j)] such that the generated SPEs seem to be robust in time and stable against thermal cycling in the investigated range of temperatures.

The possibility to deterministically generate SPEs in two-dimensional materials with very high positioning accuracy opens up

many possibilities for integrating them into optoelectronic devices and integrated quantum photonic circuits. In particular, the ability to generate SPEs on demand and in a scalable way promises integrated circuits containing a large number of SPEs, for example, multiplexed single-photon sources for applications in quantum communication or quantum sensing or fully integrated quantum photonic circuits for applications in quantum simulation such as boson sampling^{45,46} or photonic quantum computing.^{47,48}

To fabricate optoelectronic devices and integrated quantum photonic circuits, it is possible to first fabricate and encapsulate a stack of hBN/TMDC/hBN and subsequently build a nanophotonic structure around it. However, it is also possible to first fabricate a nanophotonic structure and subsequently decorate it with TMDCs and as the last step induce SPEs exactly at the desired locations with nm axial and lateral precision for controlled and optimized coupling. The latter approach has the advantage that it provides ultimate flexibility in choosing a photonic chip platform, which allows us to create hybrid systems that combine the best advantages of different worlds. For example, complex photonic circuitry is mainly achieved in silicon-based photonics due to the tremendous technological challenges in circuit fabrication.

Realizing a truly scalable platform requires the possibility to generate SPEs with good spatial and spectral matching between the emitter and the photonic structure. The first requirement, spatial matching, is met in the presented HIM irradiation approach as a spatial positioning accuracy of sub-10 nm is already demonstrated. For the spectral matching, the observed ensemble distribution of emission energies is still significantly larger than the homogeneous linewidth of a single emitter. However, the distribution is small enough such that it is possible to investigate in future works a tuning of the emission energy via static electric fields⁴⁹ or local strain.⁵⁰ Moreover, coupling the emitters to nanophotonic resonators with large quality factors and small mode volumes will enhance the emission rate via Purcell enhancement and funnel the photons into a specific mode. Finally, the generation of SPEs in 2D materials via He-ion irradiation has only been investigated with MoS₂ until now. Therefore, it is very likely that the rich class of TMDCs and other 2D materials host a large zoo of potential SPEs from which some may even be optically active spin qubits with a range of different emission wavelengths as building blocks for photonic quantum technologies.

We gratefully acknowledge financial support from the Deutsche Forschungsgemeinschaft (DFG) via the Munich Center for Quantum Science and Technology No. (MCQST)-EXC-2111-390814868 and e-conversion-EXC No. 2089/1-390776260. Moreover, we thank the European Union's Horizon 2020 research and innovation programme under Grant Agreement No. 820423 (S2QUIP), the German Federal Ministry of Education and Research via the funding program Photonics Research Germany (Contract No. 13N14846), and the Bavarian Academy of Sciences and Humanities. J.K. acknowledges support from the Alexander von Humboldt Foundation. K.D.J. acknowledges funding from the Göran Gustafsson Foundation (SweTeQ). M.L., M.F., and F.J. were supported by the Deutsche Forschungsgemeinschaft (DFG) within RTG 2247 and through a grant for CPU time at the HLRN (Göttingen/Berlin). K.W. and T.T. acknowledge support from the Elemental Strategy Initiative conducted by the MEXT, Japan, under

Grant Nos. JPMXP0112101001, JSPS KAKENHI, and JP20H00354 and the CREST (No. JPMJCR15F3), JST.

DATA AVAILABILITY

The data that support the findings of this study are available from the corresponding authors upon reasonable request.

REFERENCES

1. I. Aharonovich, D. Englund, and M. Toth, *Nat. Photonics* **10**, 631 (2016).
2. I. Aharonovich, S. Castelletto, D. A. Simpson, C.-H. Su, A. D. Greentree, and S. Praver, *Rep. Prog. Phys.* **74**, 076501 (2011).
3. R. Trivedi, K. A. Fischer, J. Vučković, and K. Müller, *Adv. Quantum Technol.* **3**, 1900007 (2020).
4. P. Senellart, G. Solomon, and A. White, *Nat. Nanotechnol.* **12**, 1026 (2017).
5. J. L. O'Brien, *Science* **318**, 1567 (2007).
6. X. He, H. Htoon, S. K. Doorn, W. H. P. Pernice, F. Pyatkov, R. Krupke, A. Jeantet, Y. Chassagneux, and C. Voisin, *Nat. Mater.* **17**, 663 (2018).
7. C. H. Bennett and G. Brassard, *Theor. Comput. Sci.* **560**, 7 (2014).
8. S. Aaronson and A. Arkhipov, in *Proceedings of the Forty-Third Annual ACM Symposium on Theory of Computing* (Association for Computing Machinery, San Jose, California, USA, 2011), pp. 333–342.
9. A. P. Lund, A. Laing, S. Rahimi-Keshari, T. Rudolph, J. L. O'Brien, and T. C. Ralph, *Phys. Rev. Lett.* **113**, 100502 (2014).
10. C. Santori, M. Pelton, G. Solomon, Y. Dale, and Y. Yamamoto, *Phys. Rev. Lett.* **86**, 1502 (2001).
11. T. Schröder, M. E. Trusheim, M. Walsh, L. Li, J. Zheng, M. Schukraft, A. Sipahigil, R. E. Evans, D. D. Sukachev, C. T. Nguyen, J. L. Pacheco, R. M. Camacho, E. S. Bielejec, M. D. Lukin, and D. Englund, *Nat. Commun.* **8**, 15376 (2017).
12. K. Ohno, F. Joseph Heremans, L. C. Bassett, B. A. Myers, D. M. Toyli, A. C. Bleszynski Jayich, C. J. Palmstrom, and D. D. Awschalom, *Appl. Phys. Lett.* **101**, 082413 (2012).
13. P. Tonndorf, R. Schmidt, R. Schneider, J. Kern, M. Buscema, G. A. Steele, A. Castellanos-Gomez, H. S. J. van der Zant, S. Michaelis de Vasconcellos, and R. Bratschitsch, *Optica* **2**, 347 (2015).
14. C. Chakraborty, L. Kinnischtzke, K. M. Goodfellow, R. Beams, and A. N. Vamivakas, *Nat. Nanotechnol.* **10**, 507 (2015).
15. A. Srivastava, M. Sidler, A. V. Allain, D. S. Lembke, A. Kis, and A. Imamoglu, *Nat. Nanotechnol.* **10**, 491 (2015).
16. M. Koperski, K. Nogajewski, A. Arora, V. Cherkez, P. Mallet, J. Y. Veuillen, J. Marcus, P. Kossacki, and M. Potemski, *Nat. Nanotechnol.* **10**, 503 (2015).
17. J. Kern, I. Niehues, P. Tonndorf, R. Schmidt, D. Wigger, R. Schneider, T. Stiehm, S. Michaelis de Vasconcellos, D. E. Reiter, T. Kuhn, and R. Bratschitsch, *Adv. Mater.* **28**, 7101 (2016).
18. C. Palacios-Berraquero, D. M. Kara, A. R.-P. Montblanch, M. Barbone, P. Latawiec, D. Yoon, A. K. Ott, M. Loncar, A. C. Ferrari, and M. Atatüre, *Nat. Commun.* **8**, 15093 (2017).
19. A. Branny, S. Kumar, R. Proux, and B. D. Gerardot, *Nat. Commun.* **8**, 15053 (2017).
20. P. Tonndorf, S. Schwarz, J. Kern, I. Niehues, O. Del Pozo-Zamudio, A. I. Dmitriev, A. P. Bakhtinov, D. N. Borisenko, N. N. Kolesnikov, A. I. Tartakovskii, S. Michaelis de Vasconcellos, and R. Bratschitsch, *2D Mater.* **4**, 021010 (2017).
21. T. T. Tran, K. Bray, M. J. Ford, M. Toth, and I. Aharonovich, *Nat. Nanotechnol.* **11**, 37 (2016).
22. T. T. Tran, C. Elbadawi, D. Totonjian, C. J. Lobo, G. Grosso, H. Moon, D. R. Englund, M. J. Ford, I. Aharonovich, and M. Toth, *ACS Nano* **10**, 7331 (2016).
23. J. Ziegler, R. Klais, A. Blaikie, D. Miller, V. R. Horowitz, and B. J. Alemán, *Nano Lett.* **19**, 2121 (2019).
24. N. V. Proscia, Z. Shotan, H. Jayakumar, P. Reddy, C. Cohen, M. Dollar, A. Alkaskas, M. Doherty, C. A. Meriles, and V. M. Menon, *Optica* **5**, 1128 (2018).
25. N. Mendelson, Z.-Q. Xu, T. T. Tran, M. Kianinia, J. Scott, C. Bradac, I. Aharonovich, and M. Toth, *ACS Nano* **13**, 3132 (2019).
26. M. E. Reimer and C. Cher, *Nat. Photonics* **13**, 734 (2019).
27. M. Ye, H. Seo, and G. Galli, *npj Comput. Mater.* **5**, 44 (2019).

- ²⁸J. Klein, M. Lorke, M. Florian, F. Sigger, L. Sigl, S. Rey, J. Wierzbowski, J. Cerne, K. Müller, E. Mitterreiter, P. Zimmermann, T. Taniguchi, K. Watanabe, U. Wurstbauer, M. Kaniber, M. Knap, R. Schmidt, J. J. Finley, and A. W. Holleitner, *Nat. Commun.* **10**, 2755 (2019).
- ²⁹J. Klein, L. Sigl, S. Gyger, K. Barthelmi, M. Florian, S. Rey, T. Taniguchi, K. Watanabe, F. Jahnke, C. Kastl, V. Zwiller, K. D. Jöns, K. Müller, U. Wurstbauer, J. J. Finley, and A. W. Holleitner, [arXiv:2002.08819](https://arxiv.org/abs/2002.08819) (2020).
- ³⁰E. Mitterreiter, B. Schuler, K. A. Cochrane, U. Wurstbauer, A. Weber-Bargioni, C. Kastl, and A. W. Holleitner, *Nano Lett.* **20**, 4437 (2020).
- ³¹M. Blauth, M. Jürgensen, G. Vest, O. Hartwig, M. Prechtel, J. Cerne, J. J. Finley, and M. Kaniber, *Nano Lett.* **18**, 6812 (2018).
- ³²F. Peyskens, C. Chakraborty, M. Muneeb, D. V. Thourhout, and D. Englund, *Nat. Commun.* **10**, 4435 (2019).
- ³³C. Errando-Herranz, E. Schöll, R. Picard, M. Laini, S. Gyger, A. W. Elshaari, A. Branny, U. Wennberg, S. Barbat, T. Renaud, M. Brotons-Gisbert, C. Bonato, B. D. Gerardot, V. Zwiller, and K. D. Jöns, [arXiv:2002.07657](https://arxiv.org/abs/2002.07657) (2020).
- ³⁴J. Wierzbowski, J. Klein, F. Sigger, C. Straubinger, M. Kremser, T. Taniguchi, K. Watanabe, U. Wurstbauer, A. W. Holleitner, M. Kaniber, K. Müller, and J. J. Finley, *Sci. Rep.* **7**, 12383 (2017).
- ³⁵F. Cadiz, E. Courtade, C. Robert, G. Wang, Y. Shen, H. Cai, T. Taniguchi, K. Watanabe, H. Carrere, D. Lagarde, M. Manca, T. Amand, P. Renucci, S. Tongay, X. Marie, and B. Urbaszek, *Phys. Rev. X* **7**, 021026 (2017).
- ³⁶O. A. Ajayi, J. V. Ardelean, G. D. Shepard, J. Wang, A. Antony, T. Taniguchi, K. Watanabe, T. F. Heinz, S. Strauf, X.-Y. Zhu, and J. C. Hone, *2D Mater.* **4**, 031011 (2017).
- ³⁷C. Pöpsel, J. Becker, N. Jeon, M. Döblinger, T. Stettner, Y. T. Gottschalk, B. Loitsch, S. Matich, M. Altzschner, A. W. Holleitner, J. J. Finley, L. J. Lauhon, and G. Koblmüller, *Nano Lett.* **18**, 3911 (2018).
- ³⁸S. Kretschmer, M. Maslov, S. Ghaderzadeh, M. Ghorbani-Asl, G. Hlawacek, and A. V. Krasheninnikov, *ACS Appl. Mater. Interfaces* **10**, 30827 (2018).
- ³⁹K. Kang, S. Xie, L. Huang, Y. Han, P. Y. Huang, K. F. Mak, C.-J. Kim, D. Muller, and J. Park, *Nature* **520**, 656 (2015).
- ⁴⁰K. F. Mak, K. He, C. Lee, G. H. Lee, J. Hone, T. F. Heinz, and J. Shan, *Nat. Mater.* **12**, 207 (2013).
- ⁴¹S. Refaely-Abramson, D. Y. Qiu, S. G. Louie, and J. B. Neaton, *Phys. Rev. Lett.* **121**, 167402 (2018).
- ⁴²H. M. Bretscher, Z. Li, J. Xiao, D. Y. Qiu, and S. Refaely-Abramson, [arXiv:2002.03956](https://arxiv.org/abs/2002.03956) (2020).
- ⁴³J. Klein, A. Kuc, A. Nolinder, M. Altzschner, J. Wierzbowski, F. Sigger, F. Kreupl, J. J. Finley, U. Wurstbauer, A. W. Holleitner, and M. Kaniber, *2D Mater.* **5**, 011007 (2017).
- ⁴⁴C. Sevik, *Phys. Rev. B* **89**, 035422 (2014).
- ⁴⁵J. C. Loredó, M. A. Broome, P. Hilaire, O. Gazzano, I. Sagnes, A. Lemaitre, M. P. Almeida, P. Senellart, and A. G. White, *Phys. Rev. Lett.* **118**, 130503 (2017).
- ⁴⁶H. Wang, J. Qin, X. Ding, M.-C. Chen, S. Chen, X. You, Y.-M. He, X. Jiang, L. You, Z. Wang, C. Schneider, J. J. Renema, S. Höfling, C.-Y. Lu, and J.-W. Pan, *Phys. Rev. Lett.* **123**, 250503 (2019).
- ⁴⁷E. Knill, R. Laflamme, and G. J. Milburn, *Nature* **409**, 46 (2001).
- ⁴⁸T. Rudolph, *APL Photonics* **2**, 030901 (2017).
- ⁴⁹J. Klein, J. Wierzbowski, A. Regler, J. Becker, F. Heimbach, K. Müller, M. Kaniber, and J. J. Finley, *Nano Lett.* **16**, 1554 (2016).
- ⁵⁰J. Q. Grim, A. S. Bracker, M. Zhalutdinov, S. G. Carter, A. C. Kozen, M. Kim, C. S. Kim, J. T. Mlack, M. Yakes, B. Lee, and D. Gammon, *Nat. Mater.* **18**, 963 (2019).